Diversity of the woodland strawberry inflorescences results from heterochrony antagonistically regulated by *FvTFL1* and *FvFT1*

Short title: Inflorescence development in strawberry

Sergei Lembinen[1], Mikolaj Cieslak[2], Teng Zhang[1], Kathryn Mackenzie[1], Paula Elomaa[1], Przemyslaw Prusinkiewicz[2*], Timo Hytönen[1*].

[1] Department of Agricultural Sciences, Viikki Plant Science Centre, University of Helsinki, P.O. Box 27, FIN-00014 Helsinki, Finland

[2] Department of Computer Science, University of Calgary, Calgary, AB T2N 1N4, Canada

[*]Correspondence:

Timo Hytönen: timo.hytonen@helsinki.fi

Przemyslaw Prusinkiewicz: pwp@ucalgary.ca

The authors responsible for distribution of materials integral to the findings presented in this article in accordance with the policy described in the Instructions for Authors (https://academic.oup.com/plcell/pages/General-Instructions) are: Timo Hytönen (timo.hytonen@helsinki.fi) and Przemyslaw Prusinkiewicz (pwp@ucalgary.ca).

.

Abstract

A vast variety of inflorescence architectures have formed during angiosperm evolution. Here we analyze the diversity and development of the woodland strawberry inflorescence. We show that it is a thyrse: a compound inflorescence in which the primary monopodial axis supports lateral sympodial branches, thus combining features of racemes and cymes. We demonstrate that this architecture is related to differences in the size and shape of the primary and lateral inflorescence meristems. We further show that woodland strawberry homologs of TERMINAL FLOWER 1 (TFL1) and FLOWERING LOCUS T (FT) antagonistically regulate the development of both the racemose and cymose components of the strawberry thyrse: the loss of functional *FvTFL1* and overexpression of *FvFT1* reduce the number and complexity of the cymose components, whereas silencing of *FvFT1* has the opposite effect and can partially rescue the *fvtfl1* mutation. We complement our experimental findings with a computational model, which captures the development of the woodland strawberry inflorescence using a small set of rules, and shows that its phenotypic diversity can be explained in terms of heterochrony resulting from the opposite action of FvTFL1 and FvFT1 on the progression from the branching to flowering state.

Key words: *Fragaria,* inflorescence, thyrse, meristem, branching, modelling, L-system, Petri net, vegetativeness,

INTRODUCTION

The arrangement of individual flowers in time and space is critical for plants' reproductive success (Harder et al., 2004; Harder & Prusinkiwicz, 2013), and ultimately for agricultural yield and fruit uniformity (Eshed & Lippman, 2019). Many angiosperms organize their flowers into clusters called inflorescences. The structural arrangement of inflorescences has long attracted the attention of plant scientists, horticulturalists, and agronomists, who described, explained, and enhanced through breeding the diverse inflorescence architectures.

Based on their branching patterns, a vast variety of inflorescence architectures can be classified as monopodial or sympodial (Weberling, 1989; Prusinkiewicz & Lindenmayer 1990). In monopodial inflorescences, or racemes (Figure 1A), new flowers form at the lateral positions on the indeterminate or determinate primary axis. In contrast, in cymose or sympodial inflorescences (Figure 1B), new flowers form at the terminal positions, and the new growth axes are established laterally. The classification of inflorescence architectures is complicated by the occurrence of compound inflorescences. For instance, panicles, or polypodial inflorescences, consist of repetitively branching determinate or indeterminate monopodial axes (Figure 1C). In contrast, in thyrses, the primary indeterminate or determinate (Prenner et al., 2009) monopodial axis bears sympodial branches (Figure 1C).

The development of inflorescence branching patterns is regulated by the activity of meristems, the small groups of multipotent cells located at the branch tips. Inflorescence meristems (IMs) are capable of initiating new IMs (i.e., branching axes) and eventually transition to flower meristems (FMs), which produce flower organs. Differences in the timing of these transitions – a form of heterochrony – control the diversity of inflorescence architectures (Grimes, 1993; Lemmon et al., 2016; Prusinkiewicz et al., 2007).

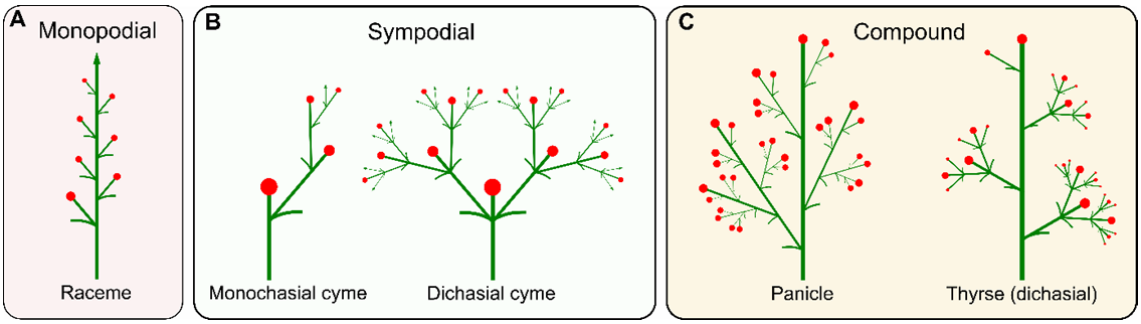

Figure 1. Inflorescence branching types. **A.** Monopodial branching of a simple raceme. **B.** Sympodial branching of monochasial and dichasial cymes. **C.** Compound branching of a panicle and a thyrse (dichasial)

The molecular processes that regulate developmental decisions in meristems have been unraveled in model plants with monopodial as well as sympodial inflorescences. In simple racemes, such as in *Arabidopsis thaliana*, the IM state is maintained by TERMINAL FLOWER 1 (TFL1). Plants lacking a functional TFL1, which is normally expressed in the center of the developing IM, produce determinate inflorescences with a few flowers (Alvarez et al., 1992; Schultz & Haughn, 1993). On the IM flanks, the expression of *LEAFY* (*LFY*) and *APETALA1* (*AP1*) activates the floral organ identity genes, promoting FM identity. Inactivation of *LFY* prevents specification of FM identity and transforms flowers into shoots (Weigel et al., 1992; Weigel & Meyerowitz, 1993).

Subsequent studies in Arabidopsis revealed that a *TFL1* homolog *FLOWERING LOCUS T* (*FT*) is also involved in regulating inflorescence architecture (Lee et al., 2019). FT and TFL1 belong to a family of phosphatidylethanolamine-binding proteins (PEBPs) and integrate environmental signals such as photoperiod and temperature to control transition to reproductive growth (reviewed in McGarry & Ayre 2012; Rantanen et al., 2015). FT is a mobile protein which is produced in leaves and moves into the shoot apical meristem (SAM) to promote flowering (Corbesier et al., 2007). In racemose Arabidopsis, the loss of functional FT promotes meristem indeterminacy and inflorescence branching (Lee et al., 2019). Further experiments revealed that FT and TFL1 proteins compete for the same binding partner, a bZIP transcription factor FD, and form complexes via 14-3-3 proteins (Zhu et al., 2021). When formed, FT-FD and TFL1-FD complexes act as transcriptional activators and

111 repressors, respectively, affecting multiple target genes including the meristem
112 identity regulators *LFY* and *AP1* (Zhu et al., 2020).

113 Studies in plants with cymose inflorescences have revealed both similarities and
114 differences in the genetic control of inflorescence development, compared to
115 racemes. For example, in petunia (*Petunia hybrida*) and tomato (*Solanum*
116 *lycopersicum*), both members of the *Solanaceae* family, the orthologs of *LFY* —
117 *FALSIFLORA* (*FA*) and *ABERRANT LEAVES AND FLOWERS* (*ALF*) — are
118 expressed in the terminal meristems and promote the transition to FM state
119 (Molinero-Rosales et al., 1999; Souer et al., 2008). However, to fully establish FM
120 identity, FA and ALF require a co-factor. In petunia, DOUBLE TOP (DOT), an
121 ortholog of UNUSUAL FLOWER ORGANS (UFO), physically interacts with ALF to
122 establish the FM identity (Souer et al., 2008). Interestingly, inactivation of *SELF-*
123 *PRUNING* (*SP*), an ortholog of *TFL1* in tomato, does not directly affect inflorescence
124 architecture (Pnueli et al., 1998). In contrast, it was shown that *FT* homolog *SINGLE*
125 *FLOWER TRUSS* (*SFT*; Molinero-Roslaes et al., 2004) regulates inflorescence
126 branching in tomato (Park et al., 2012; Quinet et al., 2006).

127 Woodland strawberry (*Fragaria vesca* L.) is a perennial rosette plant and a model for
128 the octoploid cultivated strawberry (*Fragaria* × *ananassa*) and the Rosaceae family in
129 general (Edger et al. 2018). Historically, inflorescence architecture of *Fragaria* has
130 been classified as pleiochasial cyme (Valleau, 1918), dichasial cyme (Anderson &
131 Guttridge 1982; Guttridge, 1985), cyme (Menzel, 2019) and corymb (Gleason &
132 Cronquist, 1991). This diversity of terms reflects the extensive morphological
133 variability of strawberry inflorescences, which was highlighted almost a century ago
134 (Darrow, 1929). The variability was attributed to the environment, genetic differences
135 between specific cultivars (Darrow, 1929; Foster & Janick 1969; Anderson &
136 Guttridge 1982), or to the sex of the flowers (Ashman & Hitchens, 2000). However,
137 the developmental and genetic basis of inflorescence architecture in strawberry has
138 never been elucidated.

139 Here we analyze inflorescence architecture and development in woodland
140 strawberry and begin to dissect the underlying molecular mechanism regulating its
141 development. We show that the inflorescences of woodland strawberry have
142 compound architecture, combining a monopodial primary axis with sympodial lateral

143 branches. We summarize these findings in a computational model of thyrse
144 development, which supports the diversity of strawberry inflorescence architectures
145 due to heterochrony controlled by strawberry homologs of *FT* and *TFL1*.

146 **RESULTS**

147 **Inflorescence of woodland strawberry is a determinate thyrse**

148 To understand the variability of strawberry inflorescences, we analyzed inflorescence
149 development in diploid woodland strawberry. A woodland strawberry inflorescence
150 has a monopodial primary axis terminated by a flower. This axis typically supports
151 two (Figure 2A) and occasionally three (Figure 2B) secondary branches separated
152 by long internodes. In many monopodial structures, the main axis is relatively
153 straight and can be recognized easily. In woodland strawberry, however, secondary
154 branches often assume a dominant position, continuing approximately in the
155 direction of their supporting internodes, whereas the primary axis changes direction
156 at each branching point. To identify the course of the primary axis we thus relied on
157 the positions of bracts (b; Figure 2) associated with the branches they subtend.

158 The architecture of lateral branches is different from that of the main axis. Each
159 secondary axis supports a pair of third-order branches subtended by bracts, then
160 terminates with a secondary flower. The third-order branches are approximately
161 opposite each other: the internode between them is practically absent. This
162 branching pattern repeats with each third-order branch producing a pair of fourth-
163 order branches and a terminal flower, and typically continues up to fifth- or sixth-
164 order branches. At high branching orders, only one lateral branch may emerge,
165 although both bracts are present (Jahn & Dana 1970). In spite of this departure from
166 symmetry, the structures supported by the primary axis are best characterized as
167 dichasial cymes (Figure 1B; Weberling, 1989; Prenner et al., 2009). With the
168 determinate primary monopodial axis supporting sympodial branches, inflorescence
169 of woodland strawberry qualifies as a determinate thyrse (Figure 1C).

170 Characterizing these inflorescences further, we observed that they are basitonic, i.e.,
171 the branches originating near the inflorescence base are more elaborate than those
172 near the top (Lück et al., 1990). The first lateral branch growing from the axil of the

173 leaf-like bract b1 is larger and bears more flowers than the branch that originates
174 from the axil of b2 (Figure 2, A and B). The third lateral branch, if present, is even
175 smaller and produces fewer flowers than the second or the first lateral branch. The
176 internode between b2 and b3 is also shorter than between b1 and b2 (Figure 2, A
177 and B). Moreover, the size of successive bracts is dramatically reduced, and the
178 shape is simplified from a three-lobed structure resembling a leaf to a bracteole-like
179 structure with a single lobe (Figure 2C). Within branches, the bracts are more similar
180 in shape, but also decrease in size with each successive branching iteration.

181 **Two meristem types produce determinate thyrse of woodland strawberry**

182 To investigate the ontogenesis of the strawberry inflorescence, we obtained a
183 developmental sequence of inflorescence meristems using SEM imaging (Figure 2,
184 D–M). The transition to flowering is associated with bulging and an almost two-fold
185 increase in the size of the primary inflorescence meristem (i.e., the meristem that
186 generates the primary inflorescence axis: IM1), compared to the vegetative shoot
187 apical meristem (SAM) (Figure 2, D and E). IM1 has an approximately circular cross-
188 section and produces bracts and lateral meristems (IM2) that are almost as large as
189 IM1. The first bract (b1) is initiated during the SAM to IM1 transition (Figure 2E), with
190 a lateral meristem (IM2) then forming in the bract axil (Figure 2F). As the primary
191 meristem (IM1) continues to grow, an additional one or two bracts with associated
192 lateral meristems (IM2) arise sequentially (Figure 2, G, H and N), leading to the
193 monopodial architecture of the main axis. Due to their size, these bracts and
194 meristems push the primary meristem (IM1) to the side (Figure 2O), which changes
195 the course of the main axis at each branching point (Figure 2P) as evident in the
196 mature inflorescences (e.g., Figure 2, A and B). The patterning of the main axis is
197 terminated by the primary meristem acquiring flower identity and switching to the
198 production of flower organs (FM1; Figure 2H).

199 The second and higher-order inflorescence meristems extend along the perimeter of
200 their parent meristems and have an elongated, crescent-like shape (Figure 2, F and
201 G). In consequence, the space needed to form the next-order meristems with
202 associated bracts emerges concurrently near both ends of their parent meristem
203 (Figure 2, I and J). These primordia become meristems that may produce the next
204 iteration of the same pattern, while the parent meristem continues to grow without

205 changing direction and develops into a flower (Figure 2, K–M). The compound
206 dichasial structure of the woodland strawberry inflorescence thus results.

207 However, one end of each meristem of the third order (IM3) is inevitably closer to the
208 inflorescence center than the other end, which leads to the uneven restriction of
209 space available for the development of the fourth order primordia (IM4; Figure 2Q). A
210 similar asymmetry occurs in higher order meristems, which may be the cause of, or
211 contribute to, the commonly observed departure from symmetry at high branching
212 orders, where only one lateral branch is present.

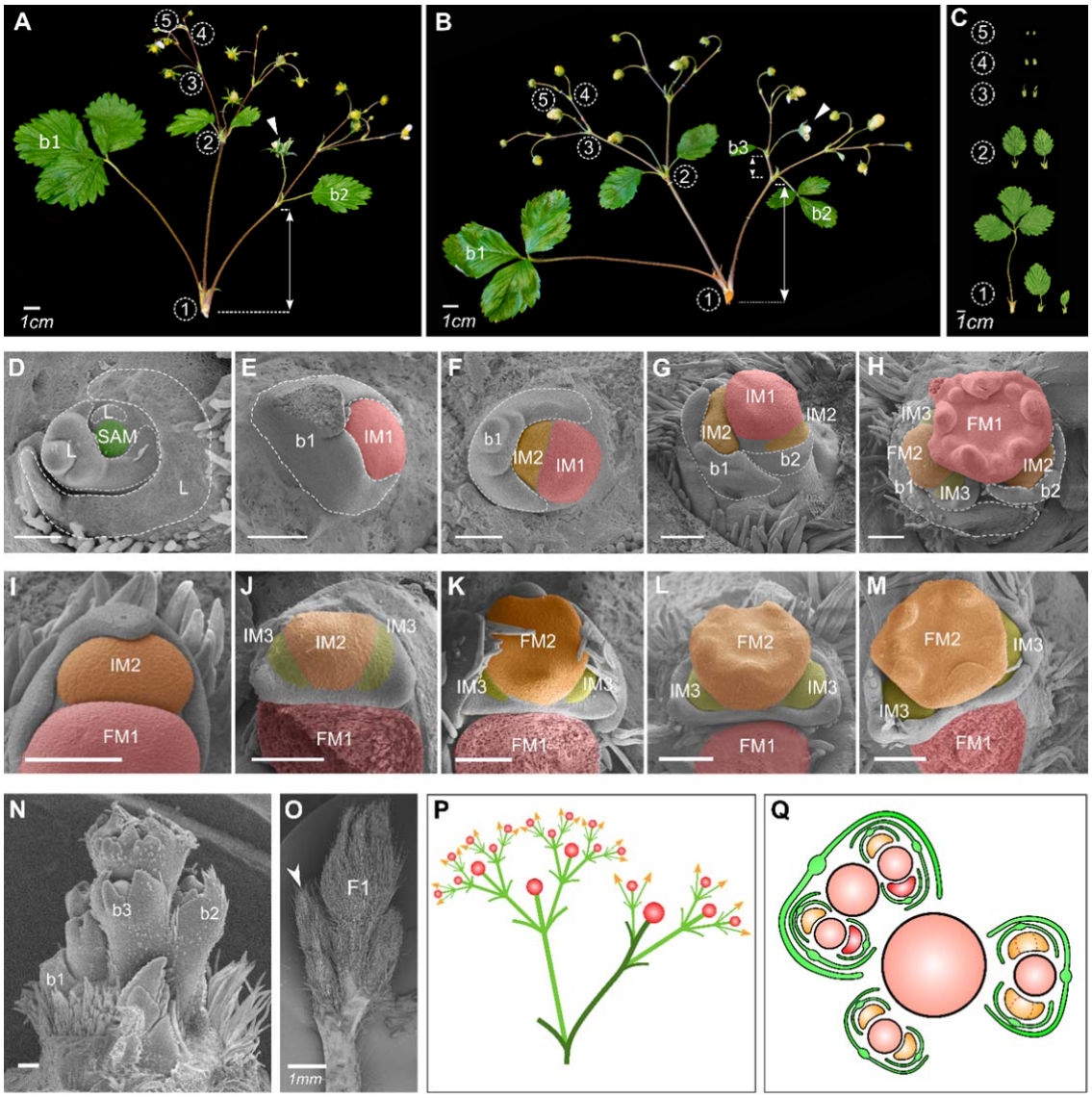

213
214 **Figure 2.** Architecture and development of thyrse inflorescence in woodland
215 strawberry. **A – B.** Inflorescence architectures of wild-type woodland strawberry
216 plants with two **(A)** and three **(B)** lateral branches on the primary axis. White
217 arrowheads indicate the primary flowers; white lines with arrows indicate the

218 distances between bracts on the primary branching axes; numbers in circles indicate
219 branching iterations **C.** Typical bract phenotypes at branching points of different
220 orders. **D–H.** Development of the primary inflorescence meristem (IM). **D.** Round
221 shoot apical meristem (SAM) with monopodially produced leaves. **E.** Early IM1 of
222 increased size, compared to the SAM. **F.** Initiation of the first lateral IM2. **G.** Initiation
223 of the second lateral IM2. **H.** IM1 transitioned into flower meristem (FM1). **I–M**.
224 Development of the lateral meristems. **I.** Elongated, crescent-like shape of IM2. **J.** An
225 almost simultaneous initiation of the lateral IM3s at the ends of IM2. **K–M.** Transition
226 of IM2 into FM2 and development of IM3s. **N.** Primary axis with three bracts, each
227 subtending a lateral meristem. **O.** The first lateral branch (white arrow) displaces the
228 primary flower (F1) and assumes a more dominant position. **P.** Schematic
229 representation of thyrse inflorescence with leading lateral branch. The primary axis is
230 highlighted in darker green. **Q.** Schematic representation of relative meristem
231 positions during the development of woodland strawberry thyrse. Relatively more
232 confined IMs are highlighted in red. Scale bars in **D–N** equal 100 µm. b – bract.
233
234

235 **FvTFL1 controls inflorescence architecture in woodland strawberry**

236 In many plant species, inflorescence architecture and flowering time are tightly
237 connected (Lee et al., 2019; Lifschitz et al., 2006; Liu et al., 2013). With this in mind,
238 we looked for the genetic regulators that can affect architecture and development of
239 the strawberry thyrse. In woodland strawberry, a mutation in *FvTFL1* accelerates
240 flowering and reverses the photoperiodic requirement for flower induction from short-
241 day to long-day (Koskela et al., 2012). To understand whether FvTFL1 also controls
242 inflorescence development in woodland strawberry, we analyzed the inflorescence
243 architecture and branching in seven *fvtfl1* mutants and nine wild type (WT)
244 genotypes collected across Europe (Supplemental Figure S1, A–C). All *fvtfl1*
245 cultivars used in this study were found to have a 2-bp deletion in the first exon of
246 *FvTFL1* (Supplemental Figure S2) putatively leading to a nonfunctional FvTFL1
247 protein.

248 We found that the number of flowers per inflorescence was reduced more than two-
249 fold in the *fvtfl1* mutant plants. On average, WT plants produced 14.2 ± 1.2 flowers
250 per inflorescence, while *fvtfl1* mutants produced only 6.5 ± 1.4 flowers per
251 inflorescence ($p < 0.0001$; Figure 3A). This reduction of flower numbers was
252 associated with changes in the general architecture of inflorescences, particularly
253 with dramatic changes in the number of lateral branches on the primary axis (Figure
254 3B—D). In plants with functional FvTFL1, we observed a high proportion of
255 inflorescences with two (72%), and three (27%), lateral branches produced on the

primary axis. Only 1% of the inflorescences had a single secondary branch. In contrast, the majority of inflorescences of *fvtfl1* mutant plants (78%) produced only one secondary branch (Figure 3C) and the remaining 22% had two secondary branches. Such a dramatic change in the proportion of lateral branches supported by the primary axis suggests that in *fvtfl1* mutants IM1 transitions to FM1 before it is able to produce the second lateral branch on the primary axis.

In the lateral cymose branches, the loss of functional FvTFL1 did not affect the dichasial branching pattern. However, the total number of branching iterations in the *fvtfl1* mutants (4.3 ± 1.1) was reduced compared to the WT plants (5.1 ± 1.0; p = 0.02; Figure 3D). To understand the reasons behind this variation we compared the bracts of *fvtfl1* mutants and WT plants (Figure 3E). The first bract (b1) on the primary axis was the largest and typically had three lobes in plants with functional and non-functional FvTFL1. Furthermore, in both groups of plants, each successive lateral IM produced smaller bracts; however, at each corresponding branching point, WT plants had larger bracts than *fvtfl1* mutants.

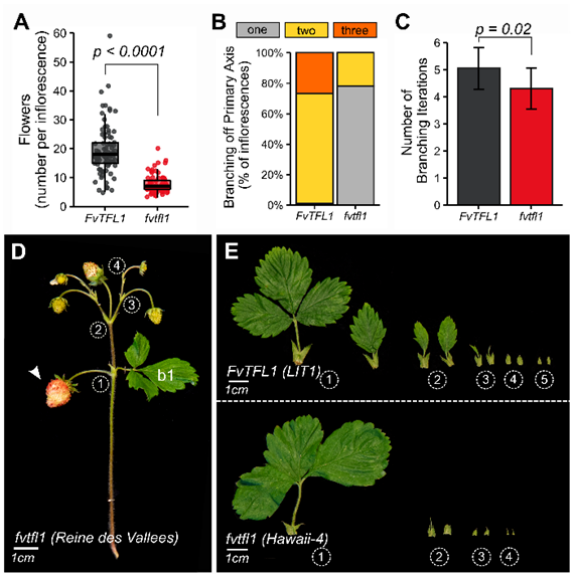

Figure 3. FvTFL1 controls inflorescence architecture in woodland strawberry. **A.** Number of flowers on the first inflorescence of seven *fvtfl1* (red) and nine *FvTFL1* (grey) genotypes. Boxplots and points show the distribution of raw data. Each point represents an individual inflorescence. **B.** Percentage of observed inflorescences with one, two, or three branches on the primary branching axis. **C.** Average number of branching iterations along the longest branching path. Bars and whiskers represent the mean ± standard deviation. Data in **A** and **C** were analyzed using a generalized linear mixed model (GLMM), with accessions and cultivars nested within *fvtfl1* and *FvTFL1* groups. P values for significant differences between *fvtfl1* and *FvTFL1* groups of plants are shown (*t*-test). **D.** Inflorescence phenotype of *fvtfl1*

282 cultivar Reine des Vallées; white arrow indicates the position of the primary flower. b
283 – bract. **E.** Typical bract phenotypes along the longest branching path of *FvTFL1* and
284 *fvtfl1* genotypes. Numbers in circles indicate branching iterations.
285
286 ***FvFT1* regulates inflorescence architecture in *fvtfl1* background**

287 Next, we decided to investigate the role of *FvFT1* in the regulation of inflorescence
288 architecture. Previously, FvFT1 was found to promote flowering under long-day
289 conditions in the *fvtfl1* mutant background (Rantanen et al., 2014; Kurokura et al.,
290 2017). We analyzed the inflorescence architecture and branching in *fvtfl1* plants
291 (*Hawaii-4*) with silenced (RNAi) and overexpressed (35S) *FvFT1* (Supplemental
292 Figure S3). Overexpression (OX) of *FvFT1* caused a pleiotropic effect by
293 dramatically reducing the overall plant and leaf size and quickly transforming all
294 shoots into inflorescences (Supplemental Figure S4). *Hawaii-4* plants typically
295 produced inflorescences with 5.7 ± 1.9 flowers, whereas transgenic plants with
296 constitutive *FvFT1* expression produced inflorescences with only 1 – 3 flowers ($p <$
297 0.0001; Figure 4, A, D and E). In contrast, silencing of *FvFT1* caused an almost two-
298 fold increase in the number of flowers per inflorescence (12 ± 0.24; $p = 0.006$; Figure
299 4A). The main reason for the higher number of flowers per inflorescence was the
300 formation of the second lateral branch along the primary axis, as in the genotypes
301 with functional FvTFL1. We observed that about 80% of the inflorescences in *FvFT1-*
302 *RNAi* plants initiated two lateral branches on the primary axis, compared to only 20%
303 in *Hawaii-4* plants (Figure 4B). Furthermore, *FvFT1-RNAi* plants typically produced
304 more branching iterations than *Hawaii-4* ($p = 0.0001$; Figure 4, C, D and F). The
305 branching of the primary axis in *fvtfl1* mutant plants (*Hawaii-4*) with silenced *FvFT1*
306 expression was similar to WT plants with functional FvTFL1, except that we did not
307 observe inflorescences with three lateral branches on the primary axis in *FvFT1-*
308 *RNAi* lines (Figure 4F). Moreover, we found that *FvFT1-RNAi* plants occasionally
309 produced an intermediate phenotype, where the second bract (b2) on the primary
310 axis was associated with the sepals of the primary flower (Figure 4G). A similar
311 phenotype was observed in the *FvFT1-OX* lines, however in these lines the first
312 bract (b1) became associated with the sepals of the primary flower (Figure 4H).

313 In the plants with the functional FvTFL1, the overexpression of *FvFT1* did not cause
314 as severe a reduction in the overall plant size (Supplemental Figure S5A) as in
315 *FvFT1-OX//fvtfl1* plants (Supplemental Figure S4). The number of flowers per

316 inflorescence of *FvFT1-OX* plants with functional FvTFL1 background was reduced
317 compared to WT and *fvtfl1* mutant plants (Supplemental Figure S3B). However, it
318 was higher than in the *FvFT1-OX* plants with *fvtfl1* background. Altogether our data
319 thus suggests the direct antagonistic functions of FvFT1 and FvTFL1 in
320 inflorescence development of woodland strawberry.

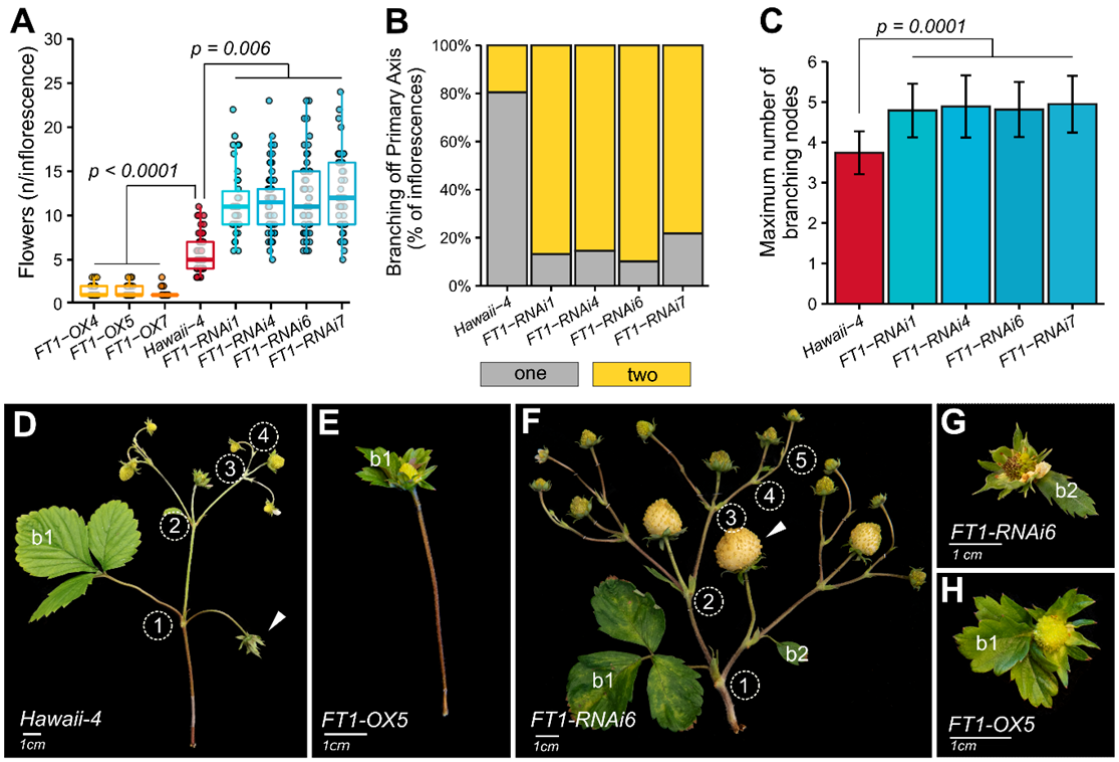

321
322 **Figure 4.** FvFT1 regulates inflorescence architecture in woodland strawberry. **A.**
323 Number of flowers per inflorescence in *FvFT1* overexpression *(FT1-OX)*, *FvFT1*
324 silenced (*FT1-RNAi*), and control *(Hawaii-4)* plants. Boxplots and points show the
325 distribution of raw data. Each point represents an individual inflorescence. Up to five
326 inflorescences per plant were examined. **B.** Maximum number of branching iterations
327 in *FvFT1-RNAi* lines and control *(Hawaii-4)* plants. Bars and whiskers show the
328 mean ± standard deviation of the raw data. Data in **A** and **B** were analyzed by fitting
329 a generalized linear mixed model (GLMM); plants were grouped within construct type
330 (OX, RNAi, or control). P values for significant differences between OX/RNAi and
331 control are shown (*t*-test). **C.** Percentage of inflorescences with one and two
332 branches along the primary axis. **D–F.** Inflorescence phenotypes of control *(Hawaii-*
333 *4), FT1-OX5* and *FT1-RNAi6* plants. The numbers in circles indicate branching
334 iterations. **G–H.** Intermediate phenotypes of *FvFT1-RNAi* and *FvFT1-OX* plants
335 associating the second (b2) or first (b1) bract of the primary axis with the sepals of
336 the primary flower. b – bract.
337

338 **FvTFL1 and FvFT1 antagonistically regulate the inflorescence architecture in**
339 **woodland strawberry**

340 To understand the mechanism of the second lateral branch formation on the primary
341 axis we analyzed WT (*FIN56*), *fvtfl1* (*Hawaii-4*) and *fvtfl1//FvFT1-RNAi* plants using
342 SEM imaging (Figure 5, A–C). We compared the WT and *fvtfl1* plants at a stage
343 when the primary FMs showed a similar developmental phase. The first lateral
344 meristem (IM2) of *FIN56* with functional FvTFL1 was at a later developmental stage
345 (Figure 5A) than the first (and single) lateral meristem (IM2) of *Hawaii-4* (Figure 5B).
346 In *FIN56*, the lateral IM2 already formed a pair of axillary meristems (IM3s) and sepal
347 primordia, while in *Hawaii-4*, only the bracts could be clearly distinguished on the
348 single lateral IM2. A similar difference was also evident when *FvFT1* was silenced in
349 *fvtfl1* background (Figure 5C). Overall, these findings suggest that the primary IM1 of
350 the plants with functional FvTFL1 or silenced *FvFT1* develops into FM1 slower than
351 in *fvtfl1* mutants, thus allowing formation of additional bracts and lateral IM2s.

352 In woodland strawberry, *FvTFL1* is highly expressed in the vegetative shoot apex
353 and gradually downregulated during flowering induction (Koskela et al. 2012).
354 Molecular antagonism between *TFL1* and *LFY* has been described as the
355 mechanism controlling inflorescence architecture in Arabidopsis (Schultz & Haughn,
356 1993). Subsequent studies in other species found that *AP1* may substitute *LFY* as
357 *TFL1* antagonist in inflorescence development (Kobayashi et al., 2012; Ma et al.,
358 2017). Here we observed that the decrease of *FvTFL1* expression is associated with
359 the progression of the vegetative SAM towards FM identity (Figure 5D). The
360 expression of the strawberry homologs of *LFY* and *AP1* showed the opposite pattern
361 (Figure 5, E and F). The expression of both *FvLFYa* (*FvH4_5g09660*) and *FvAP1*
362 (*FvH4_6g29600*) began increasing in late IM1s, where *FvTFL1* was still present.
363 *FvTFL1* had the lowest expression in the FM tissues, concordant with the highest
364 expression of *FvLFYa* and *FvAP1*. Altogether, our data suggests that the role of
365 TFL1 in maintaining IM identity (Alvarez et al., 1992; Schultz & Haughn, 1993) is
366 conserved in woodland strawberry.

367 To further elucidate the mechanism by which FvFT1 regulates inflorescence
368 architecture in the absence of functional FvTFL1, we analyzed the expression levels
369 of *FvTFL1, FvLFYa* and *FvAP1* in the SAMs of *FIN56* (*FvTFL1*)*, Hawaii-4* (*fvtfl1*) and

370 *FvFT1-RNAi* (*fvtfl1*) plants. We observed that the expression of *FvLFYa* and *FvAP1*
371 was lower in the SAMs of *FIN56* and *FvFT1-RNAi* plants compared to *fvtfl1* (*Hawaii-*
372 *4*) (Figure 5, H and J). In addition, the expression of *FvTFL1* was the lowest in the
373 *fvtfl1* mutant (Figure 5G). Our results thus suggest that FvTFL1 and FvFT1
374 antagonistically control the transition to FM identity by regulating the expression of
375 *FvLFYa* and *FvAP1*.

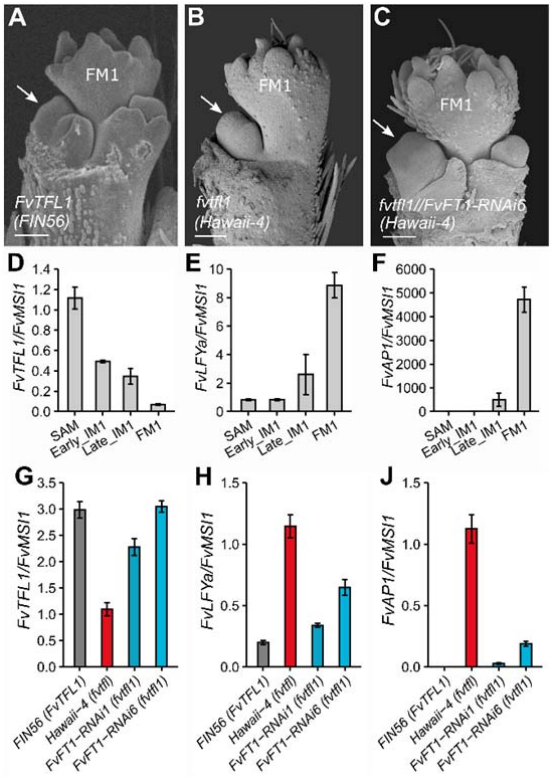

376
377 **Figure 5.** FvTFL1 and FvFT1 antagonistically shape the inflorescence of woodland
378 strawberry. **A–C.** Primary axis development in *FvTFL1 WT* **(A)**, *fvtfl1* mutant **(B)**, and
379 *FvFT1-RNAi* **(C)** plants. White arrows denote the first lateral IM2. Scale bars equal
380 100μm. **D–F.** The expression pattern of *FvTFL1* **(D)***, FvLFYa* **(E)***, and FvAP1* **(F)** in
381 different meristems of *FvTFL1 WT* (*FIN56*) during transition to flowering. **G–J.** The
382 expression pattern of *FvTFL1* **(G)**, *FvLFYa* **(H)**, and *FvAP1* **(J)** in the SAMs of FIN56
383 (WT), *Hawaii-4* (*fvtfl1*) and *FvFT1-RNAi* (*Hawaii-4*) plants. Bars and whiskers show
384 the mean ± standard error (n = 3 – 5). Expression levels were normalized to SAM (D
385 –F) or *Hawaii-4* (G–J). *FvMSI1* was used as a calibrator gene.
386

387 **A computational model supports heterochrony as the key determinant of the**
388 **strawberry inflorescence diversity**

389 We constructed a parametrized computational model of the woodland strawberry
390 inflorescence to show that the observed diversity of the inflorescence architecture

391 can be attributed to the regulation of the rate of development by *FvTFL1* and *FvFT1*.
392 The model is expressed as an L-system, with separate rules capturing the
393 monopodial development of the primary axis and the sympodial development of
394 branches. Generic rules for both types of branching (c.f. Prusinkiewicz &
395 Lindenmayer, 1990) are extended with a mechanism that controls transitions of
396 individual meristems to flowers and terminates the formation of new meristems at the
397 end of inflorescence development. These processes are controlled by a synthetic
398 variable (integrating many influences) called *vegetativeness* (*veg*) (Prusinkiewicz et
399 al., 2007), which is related to the concepts of a controller of phase switching (Schultz
400 and Haughn, 1993) and meristem maturation (Park et al., 2012). In the strawberry
401 model, *veg* decreases monotonically with time (Figure 6A). Its values are compared
402 to two thresholds, th_m and th_s, which are pertinent to the fate of monopodial and
403 sympodial meristems, respectively. As long as $veg \geq th_m$, the primary meristem
404 periodically produces lateral primordia subtended by bracts (Event 1 in Figure 6B[*]).
405 This process terminates when *veg* drops below th_m, at which point the meristem
406 produces a terminal flower (Event 2). A lateral primordium develops in turn into a
407 lateral meristem supported by a bract (Event 3), which subsequently produces two
408 next-order primordia and a terminal flower (Event 4). This process periodically
409 iterates as long as $veg \geq th_s$, giving rise to a compound dichasial cyme. Eventually
410 *veg* drops below th_s, which results in the production of bracts without associated
411 meristems (Event 5) and arrests further branching. The distinct development of
412 branches originating at the same node, in particular the case when only one lateral
413 branch is present, are captured by introducing a small difference in the value of
414 threshold th_s between sibling meristems. This difference may be related to the
415 unequal space available for the development of primordia on opposite sides of an
416 elongated meristem (Figure 2Q).

417 In addition to the thresholds controlling branching architecture, the model includes
418 thresholds bth_1 and bth_2 (Figure 6A), which control the transition of bracts from the 3-
419 lobed form to 1-lobed form and to narrow scales, respectively. The model also
420 includes a number of parameters and growth functions that control the geometry of

[*] The concept of Petri nets formally underlying Figure 6B is further described by Peterson (1981), and in application to plant modeling by Prusinkiewicz and Remphrey (2000). The use of Petri nets enhances the flowchart representation of inflorescence development proposed by Kellogg (2000) by explicitly representing events that produce multiple organs, which then develop concurrently.

the phenotypes of interest. Parameter values and functions can be chosen such that the simulated inflorescence development (Supplemental Movie 1) closely approximates observations (Figure 7). In particular, the deviation of the primary axis from a straight course substantially affects the overall appearance of the inflorescence, obscuring its thyrsoid architecture (Figure 6C). For details see the supplemental Model Code, Model Description, and the parameter values listed in Supplemental Table S2.

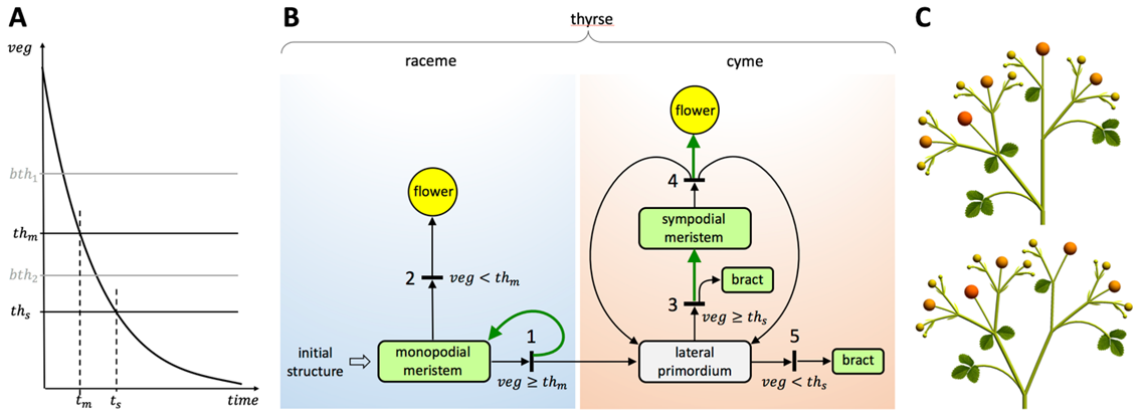

Figure 6. Developmental model of a woodland strawberry thyrse. **A**. Control of a thyrse development by *vegetativeness* (*veg*). Crossing threshold th_m terminates the production of primordia by the primary (monopodial) meristem; crossing threshold th_s terminates production of lateral primordia by the sympodial meristems. Times th_m and th_s at which these thresholds are crossed determine the inflorescence complexity (extent of branching). Additional thresholds, *bth*1 and bth_2, control the transitions of bracts from 3-lobed to 1-lobed to narrow-scale forms. **B.** Petri net representation of the meristem production and fate. Circles and rectangles represent plant organs. The term "lateral primordium" denotes an incipient structure yielding a lateral meristem supported by a bract, or a bract alone. Short black bars represent events taking place during development. These events are labelled by a number and are associated with conditions under which they may take place. Arcs with arrows represent relations between these events and the resulting structures. Two arrows originating in the same rectangle indicate alternative organ fates. Two or three arrows emanating from the same bar indicate production of multiple organs. Green-colored arrows indicate the introduction of an internode. **C**. The impact of the monopodial axis course on thyrse geometry. In the top model the monopodial axis is straight; in the bottom it deviates in the direction opposite to the lateral branch, as commonly observed in woodland strawberry (c.f. Figure 2 A, B, O and P).

Figure 7. Development of a woodland strawberry inflorescence. **A.** Snapshots of inflorescence growth in a WT (GER12 x FIN2) woodland strawberry. Photographs were taken with the inflorescence supported in a vertical position to expose the branching pattern. Plants were induced to flower under 11°C and a 12h/12h (day/night) photoperiod for 6 weeks, then moved to 17°C and a 18h/6h photoperiod during inflorescence growth. Numbers indicate days of observation. **B.** Simulated development calibrated to sequence (A).

We experimented with the model to capture the key inflorescence features of the plants with different constitutions of *FvTFL1* and *FvFT1*. The most prominent trait that distinguishes the architectures collected in Figure 8A is the decreasing complexity (maximum order) of branching, caused by an accelerated cessation of branching. This decrease is accompanied by the accelerated progression of bracts from the three-lobed leaf-like form at the most basal position to the one-lobed and small-scale forms at more distal positions. Both the branching architecture and bract form are controlled in the model by the initial value and rate of decline of *veg*, and the thresholds th_m, th_s, bth_1, and bth_2 with respect to *veg* (Figure 6A). We observed that the sequence of inflorescence architectures (branching topologies) presented in Figure 8A can be reproduced simply by gradually increasing the rate of decline of *veg*, with minimal adjustments to other parameters except for the extreme phenotype of the *fvtfl1//FvFT1-OX* plants (Figure 8B; Supplemental Movies 2–8; Supplemental Table S1). A similar effect is caused by gradually reducing the initial value of *veg*. This result supports the conclusion that the diversity of strawberry inflorescences is a

473 manifestation of heterochrony, in which *FvTFL1* decelerates, and *FvFT1* accelerates
474 the rate of *veg* decline, respectively.

475
476 **Figure 8.** Diversity of woodland strawberry inflorescence phenotypes can be
477 reproduced by altering model parameters. **A.** Observed diversity of inflorescence
478 phenotypes. Scale bar equals 1 cm. **B.** Phenotypes reproduced by the model. Lines
479 with text describe the genetic constitution of the plants. The color of the line indicates
480 the rate of *veg* decline (green – slower, red – faster).
481

482 **DISCUSSION**

483 Almost a century ago, Darrow (1929) pointed out the extensive variability of
484 inflorescence architectures in cultivated strawberry *(F. × ananassa)* varieties, which
485 he attributed to genetic differences between cultivars, environmental factors, and the
486 vigor of individual plants. As outlined in Darrow's inflorescence diagrams, the
487 variation in inflorescence architecture of strawberries is mainly due to the variable
488 number of branches on the primary inflorescence axis and branching iterations in the
489 lateral branches. Here, using diploid woodland strawberry, we established the
490 developmental and genetic basis of this variation. We have shown that the
491 inflorescences of woodland strawberry consist of a monopodial determinate primary
492 axis supporting sympodial lateral branches, an architecture characterized as a
493 determinate thyrse (Prenner et al., 2009). This architecture arises from differences
494 between the primary and lateral inflorescence meristems.

495 We have further demonstrated that the number of lateral branches on the primary
496 monopodial axis and the number of iterations in the lateral sympodial branches are

497 oppositely controlled by the two PEBP family proteins FvTFL1 and FvFT1. These
498 proteins act by changing the timing of developmental decisions that transition
499 inflorescence meristems to the flowering state, and eventually terminate the
500 formation of further meristems. We supported this observation with a computational
501 model which captures the diversity of studied phenotypes.

502

503 **Two types of IMs produce thyrse inflorescence in woodland strawberry**

504 In the ontogenic view of inflorescence diversity, distinct inflorescence architectures
505 are produced by different types of meristems (Claßen-Bockhoff & Bull-Hereñu,
506 2013). Our data shows that the determinate thyrse of woodland strawberry, which
507 combines monopodial and sympodial branching patterns, is produced by two types
508 of IMs. The monopodial primary axis is produced by a primary IM (IM1), which
509 originates from the SAM that has expanded and begun producing leaf-like bracts
510 upon entering the reproductive phase. Like the SAM, IM1 has a circular cross-
511 section and produces bracts acropetally. After producing one to three bracts, the
512 primary IM acquires FM identity, thus forming a closed monopodial axis. Each of the
513 bracts on the monopodial axis subtends the newly formed and rapidly growing lateral
514 IM, which, unlike the primary IM, has a crescent-shaped cross-section. According to
515 the first available space theory (Hofmeister, 1868), new organ primordia are initiated
516 in the largest available space between the previous ones. The initially elongated
517 shape of the lateral IMs thus promotes a dichasial branching pattern, by allowing the
518 pairwise initiation of next-order bracts and branches near opposite ends of the
519 meristem.

520 We observed that, despite their morphological differences, both types of IMs
521 followed a similar developmental progression towards FMs. Moreover, along the
522 monopodial axis and with each successive branching iteration, the leaf-like bracts
523 and the internodes were gradually reduced. By associating this reduction with the
524 monotonic decrease of *veg*, properly choosing thresholds th_m and th_s at which the
525 activity of each type of IM terminates, and setting additional parameters (e.g.,
526 branching angles) to agree with the observation of reference plants, we have been
527 able to model the development of the woodland strawberry thyrse. The model

528 confirms the usefulness of *veg* as a controller of development and sets the stage for
529 understanding the diversity of strawberry inflorescences.

530 **_FvTFL1_ and _FvFT1_ antagonistically regulate the complexity of woodland**
531 **strawberry inflorescences**

532 Previous studies uncovered the role of *FvTFL1* in the regulation of flowering time in
533 woodland strawberry (Koskela et al., 2012; Koskela et al., 2017). Flowering in WT
534 strawberry requires downregulation of *FvTFL1*, which triggers the expression of the
535 FM identity gene *FvAP1* (Koskela et al., 2012). Our results further show that *FvTFL1*
536 is gradually downregulated as the SAM progresses towards the IM and then to the
537 FM state. This expression pattern is different from that previously described in
538 racemose and cymose plants. In monopodial Arabidopsis, *TFL1* is expressed in the
539 SAM and IM and is specifically required to maintain IM identity (Alvarez et al., 1992;
540 Schultz & Haughn, 1993). In sympodial tomato, *SP* - the closest homolog of *TFL1* -
541 is expressed only in vegetative axillary meristems (Pnueli et al., 1998; Thouet et al.,
542 2012). Concordantly, the *tfl1* mutation in Arabidopsis leads to the formation of a
543 terminal flower on the otherwise indeterminate IM, whereas *sp* mutants in tomato do
544 not show alterations of inflorescence architecture. The determinate primary IM of
545 woodland strawberry is related to Arabidopsis in the sense that the loss of functional
546 *FvTFL1* accelerates the formation of the terminal flower and cessation of the
547 formation of lateral meristems. As a result, only one lateral branch is formed on the
548 primary monopodial inflorescence axis of the *fvtfl1* mutant. Furthermore, in the lateral
549 sympodial branches, the maximum number of branching iterations is reduced in the
550 *fvtfl1* mutant plants, consistent with the accelerated termination of IMs.

551 Mutations in *FT* homologs were shown to affect the architecture in both monopodial
552 and sympodial inflorescences. In Arabidopsis, FT, and its close homolog TSF,
553 promote FM identity transition and act antagonistically to TFL1 (Lee et al., 2019).
554 Furthermore, mutation in *SFT* was found to promote inflorescence branching in
555 tomato (Park et al., 2012), suggesting a similar function. In woodland strawberry,
556 FvFT1 was previously shown to promote flowering in *fvtfl1* mutant background
557 (Koskela et al., 2012; Rantanen et al., 2014). Here we found that the role of *FvFT1* in
558 inflorescence development of woodland strawberry is antagonistic to that of *FvTFL1*.
559 Our data suggests that the faster progression towards FM in the *fvtfl1* mutant plants
560 may be delayed or further accelerated by altering the expression of *FvFT1*.

561 Silencing *FvFT1* partially compensated for the lack of functional FvTFL1, as we
562 observed an increased percentage of inflorescences with two lateral branches on the
563 primary axis and an increased number of branching iterations. In contrast, the
564 ectopic *FvFT1* expression in the *fvtfl1* mutants caused pleiotropic changes in plant
565 architecture by inducing flowering in young seedlings, thus reducing overall plant
566 size, and resulting in inflorescences with only a few flowers. Furthermore, in the
567 functional FvTFL1 background, the overexpression of *FvFT1* resulted in an
568 inflorescence phenotype intermediate between *fvtfl1* and *fvtfl1//FvFT1-OX*, in line
569 with the proposed antagonistic function of these genes.

570 Recently it was shown that the mutation of *FvLFYa* in woodland strawberry causes
571 the homeotic conversion of flower organs into bracts and the production of additional
572 flowers (Zhang et al., 2022), indicating a conserved function for specifying FM
573 identity. In Arabidopsis and rice, FT and TFL1 proteins are known to competitively
574 bind to bZIP transcription factor FD and 14-3-3 proteins (Zhu et al., 2021; Kaneko-
575 Suzuki et al., 2018). When formed, the FT-FD complex was found to act as a
576 transcriptional activator of *LFY* and *AP1*, whereas TFL1-FD was found to act as a
577 repressor (Zhu et al., 2021). In our experiments, both *FvLFYa* and *FvAP1* were
578 downregulated in the plants with either functional FvTFL1 or silenced *FvFT1* in *fvtfl1*
579 background, suggesting a similar regulatory mechanism.

580 Altogether, our experimental data indicate that FvTFL1 and FvFT1 antagonistically
581 regulate the complexity of the woodland strawberry inflorescence architecture. With
582 the help of a computational model, we have further shown that the observed diversity
583 of strawberry architectures can be attributed to heterochrony, where FvTFL1 delays,
584 and FvFT1 accelerates the cessation of branching and the production of flowers.

585

586 **MATERIALS AND METHODS**

587 **Plant material**

588 Nine *Fragaria vesca* and seven *F. vesca semperflorens* (*fvtfl1* mutant) accessions
589 were used in this study (Supplemental Table S2). Previously reported *FvFT1*
590 overexpression (OX) and RNA silencing (RNAi) lines in *fvtfl1* (*Hawaii-4*) background
591 were used (Koskela et al., 2012; Rantanen et al., 2014). The specificity of the RNAi
592 construct to *FvFT1* was confirmed by analyzing the expression of *FvFT2* and *FvFT3*
593 in the FM tissues (Supplemental Figure S6A – B). To obtain *FvFT1-OX* plants in
594 *FvTFL1* background, we crossed *FvFT1-OX5 (Hawaii-4)* line with *FvTFL1* accession
595 *(FIN56)* and self-pollinated the progeny. F_2 plants carrying FIN56 *FvTFL1* allele and
596 the desired *FvFT1* construct were used in the experiments.

597 **Growth conditions and phenotyping**

598 All plants were grown in greenhouse conditions with controlled temperature and
599 photoperiod. In the greenhouse, the plants were illuminated with 150µmol m^{-2} s^{-1}
600 light intensity using high-pressure sodium lamps (Airam 400W, Kerava, Finland).
601 Germinated from seeds or clonally propagated plants were first potted into 7x7cm
602 plastic pots filled with peat moss (Kekkilä, Finland), and kept in the greenhouse
603 under plastic covers for two weeks. Plants were pre-grown at 18°C and an 18h
604 photoperiod for four - six weeks, and periodically supplemented with fertilizer (NPK
605 17-4-25; Kekkilä). Plants were then potted into 13cm Ø pots and grown until the
606 inflorescences were fully formed. Plants were irrigated with tap water supplemented
607 with fertilizer (NPK 17-4-25; Kekkilä)

608 For the analysis of FvFT1 and FvTFL1 functions we pre-grew 8 – 13 seed
609 germinated plants per transgenic line or cultivar, or 6 – 13 clonally propagated plants
610 per accession with functional FvTFL1, in growth rooms under an 18h/6h (day/night)
611 photoperiod (AP67, Valoya, Finland) and 25°C temperature. For floral induction, the
612 plants were then moved to a 12h/12h (day/night) photoperiod at 18°C in the
613 greenhouse for six weeks. After the treatment, the plants were kept under 18°C and
614 an 18h/6h (day/night) photoperiod until the inflorescences were fully developed.
615 Inflorescence architecture was analyzed by counting the total number of flowers and
616 flower buds, the number of branching iterations in the longest branching path, and

617 the number of branches on the primary axis. For the functional analysis of FvTFL1,
618 the first fully developed inflorescence was analyzed from each plant. For the
619 functional analysis of FvFT1, five fully developed inflorescences were analyzed.

620 **Genotyping**

621 DNA was extracted from young, folded leaves of *fvtfl1* mutants and WT plants listed
622 in Supplemental Table S2 as in Koskela et al. (2012). PCR amplified *FvTFL1*
623 fragments were excised from agarose gel, purified, and sequenced using primers
624 listed in Supplemental Table S3.

625 **RNA extraction and qPCR analysis**

626 Meristems were dissected under stereomicroscope (Zeiss Stemi 2000). SAMs, IMs,
627 and FMs were excised and collected into separate Eppendorf tubes. 5 – 10
628 meristems were pooled into one tube and used for RNA extraction. Total RNA was
629 extracted from pooled meristem samples as in Mouhu et al. (2009) and treated with
630 rDNase (Macherey-Nagel GmbH, Düren, Germany). 500ng of total RNA was used
631 for cDNA synthesis using ProtoScriptII reverse transcriptase. RT-PCR was
632 performed using a LightCycler 480 SYBR Green I Master kit (Roche Diagnostics,
633 Indianapolis, US) and a Roche LightCycler (Roche Diagnostics, Indianapolis, US)
634 with three technical replicates for each of the tested genes. *FvMSI1 (FvH4_7g08380)*
635 was used as a reference gene. The qPCR primers used in this study are listed in
636 Supplemental Table S3.

637 **SEM imaging**

638 Dissected meristem samples were fixed in an FAA buffer (3.7 % formaldehyde 5 %
639 acetic acid, and 50 % ethanol) overnight and transferred through ethanol series (50
640 %, 60%, 70 %, 80 %, 90 %, 100%, 100 %) under mild vacuum (~0.6 atm). Critical
641 point drying was done using a Leica EM CPD300 (Leica Mikrosystems GmbH,
642 Vienna, Austria). The dried samples were then coated with platinum by a Quorum
643 Q150TS coater (Quorum Technologies, UK). The samples were examined under a
644 Quanta 250 FEG (FEI, Hillsboro, OR, USA) scanning electron microscope located at

645 the Electron Microscopy Unit (Institute of Biotechnology, University of Helsinki).
646 Pseudo-coloring was done in Adobe Photoshop CC 2019.

647 **Statistical analyses**

648 The phenotypic data (flowering time, number of flowers per inflorescence and
649 branching iterations) were analyzed using random intercept models, $y = \beta_0 + \beta_1 X +$
650 $Gt + \varepsilon$, where y = dependent variable, βs = fixed effects, X = design matrices for
651 *FvTFL1* background or *FvFT1* transgenic construct, Gt = random accession or
652 independent line effect, and ε = an error term. Poisson distribution model was
653 applied for count data. Statistical analyses were performed using the R/lme4
654 package (Bates et al., 2015). All analyses were performed in R version 4.1.1 (R Core
655 Team 2021).
656

657 **Inflorescence modelling**

658 The models were written in the L-system-based L+C plant modeling language
659 (Karwowski and Prusinkiewicz, 2003) and executed using the lpfg simulator
660 incorporated into the Virtual Laboratory (vlab) v5.0 plant modeling software
661 (algorithmicbotany.org/virtual_laboratory). All simulations were performed on
662 MacBook Pro computers under macOS High Sierra 10.13.6. The supplemental
663 materials include three complete vlab objects (versions of the model): the basic
664 version with a simplified representation of plant organs (bracts and flowers),
665 convenient for analyzing the model logic; the extended version with full
666 representation of organs, used in the model calibration shown in Figure 7; and the
667 same extended version configured to simulate the diverse phenotypes shown in
668 Figure 8. The key elements of the model code are discussed in the Supplemental
669 Model Description. Parameters used to simulate the diverse phenotypes were found
670 by interactively exploring the model parameter space using the tools included in vlab
671 (control panels and graphically defined timelines and functions). The reference
672 model (Figure 7) was calibrated using the method described by Cieslak et al. (2022).
673

674 **Acknowledgements**

675 We thank Elli Koskela for providing seeds; Eija Takala and Marjo Kilpinen for
676 laboratory assistance; Katriina Palm for maintaining the plant materials; the staff of
677 the Electron Microscopy Unit at the Institute of Biotechnology, University of Helsinki,

for assistance. This work was supported by Jane and Aatos Erkko Foundation grant 4709012 (to P.E. and T.H.), the Academy of Finland grant 317306 (to T.H), Natural Sciences and Engineering Research Council of Canada Discovery Grant 2019-06279 (to P.P.), the Plant Phenotyping and Imaging Research Centre/Canada First Research Excellence Fund (to P.P. and M.C.), and the Finnish Cultural Foundation grant 00221168 (to S.L.). S.L. was affiliated with the Doctoral Programme in Plant Sciences (DPPS, University of Helsinki).

REFERENCES

Alvarez J, Guli CL, Yu X-H, Smyth DR (1992) *terminal flower*: a gene affecting inflorescence development in *Arabidopsis thaliana*. Plant J **2:** 103–116

Anderson HM, Guttridge CG (1982) Strawberry truss morphology and the fate of high-order flower buds. Crop Research **22:** 105–122

Ashman TL, Hitchens MS (2000) Dissecting the causes of variation in intra-inflorescence allocation in a sexually polymorphic species, *Fragaria virginiana* (Rosaceae). Am J Bot **87:** 197–204

Bates D, Mächler M, Bolker B, Walker S (2015) Fitting linear mixed-effects models using lme4. J Stat Softw **67:** 1–48

Cieslak M, Khan N, Ferraro P, Soolanayakanahally R, Robinson SJ, Parkin I, McQuillan I, Prusinkiewicz P (2022) L-system models for image-based phenomics: case studies of maize and canola. isP **4:** diab039

Claßen-Bockhoff R, Bull-Hereñu K (2013) Towards an ontogenetic understanding of inflorescence diversity. Ann Bot **112:** 1523–1542

Corbesier L, Vincent C, Jang S, Fornara F, Fan Q, Searle I, Giakountis A, Farrona S, Gissot L, Turnbull C, Coupland G (2007) FT protein movement contributes to long-distance signaling in floral induction of *Arabidopsis*. Science **316:** 1030–1033

Darrow GM (1929) Inflorescence types of strawberry varieties. Am J Bot **16:** 571–585

Edger PP, VanBuren R, Colle M, Poorten TJ, Wai CM, Niederhuth CE, Alger EI, Ou S, Acharya CB, Wang J, Callow P, McKain MR, Shi J, Collier C, Xiong Z, Mower JP, Slovin JP, Hytönen T, Jiang N, Childs KL, Knapp SJ (2018) Single-molecule sequencing and optical mapping yields an improved genome of woodland strawberry (*Fragaria vesca*) with chromosome-scale contiguity. GigaScience **7:** gix124

Eshed Y, Lippman ZB (2019) Revolutions in agriculture chart a course for targeted breeding of old and new crops. Science **366:** eaax0025

Foster JC, Janick J (1969) Variable branching patterns in the strawberry inflorescence. J Am Soc Hortic Sci **94:** 440–443

715 **Gleason HA, Cronquist A** (1991) *Manual of Vascular Plants of Northeastern United*
716 *States and Adjacent Canada* (2nd ed.). New York Botanical Garden

717 **Grimes J** (1999) Inflorescence morphology, heterochrony, and phytogeny in the
718 mimosoid tribes ingeae and acacieae (Leguminosae: Mimosoideae). Bot Rev **65:**
719 317–347

720 **Guttridge CG** (1985) *Fragaria x ananassa*. *In* AH Halevy ed, Handbook of Flowering, v*ol.*
721 ***3.*** CRC Press, Boca Raton, FL, pp 16–33

722 **Harder LD, Jordan CY, Gross WE, Routley MB** (2004) Beyond floricentrism: the
723 pollination function of inflorescences. Plant Species Biol **19:** 137–148

724 **Harder LD, Prusinkiewicz P** (2013) The interplay between inflorescence development
725 and function as the crucible of architectural diversity. Ann Bot **112:** 1477–1493

726 **Hofmeister W** (1868) Allgemeine Morphologie der Gewächse. *In* A de Bary, TH Irmisch,
727 J Sachs, eds. Handbuch der Physiologischen Botanik. Engelmann, Leipzig, pp 405 –
728 664

729 **Jahn OL, Dana MN** (1970) Crown and inflorescence development in the strawberry,
730 *Fragaria ananassa*. Am J Bot **57:** 605–612

731 **Kaneko-Suzuki M, Kurihara-Ishikawa R, Okushita-Terakawa C, Kojima C, Nagano-**
732 **Fujiwara M, Ohki I, Tsuji H, Shimamoto K, Taoka KI** (2018) TFL1-like proteins in
733 rice antagonize rice FT-like protein in inflorescence development by competition for
734 complex formation with 14-3-3 and FD. Plant Cell Physiol **59:** 458–468

735 **Karwowski R, Prusinkiewicz P** (2003) Design and implementation of the L+C modeling
736 language. Electron Notes Theor Comput Sci **86:** 134–152

737 **Kellogg EA** (2000) A model of inflorescence development. *In* KL Wilson and DA
738 Morrison eds, Monocots: Systematics and Evolution. CSIRO, Melbourne, pp 84–88.

739 **Kobayashi K, Yasuno N, Sato Y, Yoda M, Yamazaki R, Kimizu M, Yoshida H,**
740 **Nagamura Y, Kyozuka J** (2012) Inflorescence meristem identity in rice is specified
741 by overlapping functions of three *AP1*/*FUL*-Like MADS box genes and *PAP*2, a
742 *SEPALLATA* MADS box gene. Plant Cell **24:** 1848–1859

743 **Koskela EA, Mouhu K, Albani MC, Kurokura T, Rantanen M, Sargent DJ, Battey NH,**
744 **Coupland G, Elomaa P, Hytönen T** (2012) Mutation in *TERMINAL FLOWER1*
745 reverses the photoperiodic requirement for flowering in the wild strawberry *Fragaria*
746 *vesca*. Plant Physiol **159:** 1043–1054

747 **Koskela EA, Kurokura T, Toivainen T, Sønsteby A, Heide OM, Sargent DJ, Isobe S,**
748 **Jaakola L, Hilmarsson H, Elomaa P, Hytönen T** (2017) Altered regulation of
749 *TERMINAL FLOWER 1* causes the unique vernalisation response in an arctic
750 woodland strawberry accession. New Phytol **216:** 841–853

751 **Kurokura T, Samad S, Koskela E, Mouhu K, Hytönen T** (2017) *Fragaria vesca*
752 CONSTANS controls photoperiodic flowering and vegetative development. J Exp Bot
753 **68:** 4839–4850

754 **Lee C, Kim S-J, Jin S, Susila H, Youn G, Nasim Z, Alavilli H, Chung K-S, Yoo SJ,**
755 **Ahn JH** (2019) Genetic interactions reveal the antagonistic roles of *FT/TSF* and
756 *TFL1* in the determination of inflorescence meristem identity in Arabidopsis. Plant J
757 **99:** 452–464

758 **Lemmon ZH, Park SJ, Jiang K, Van Eck J, Schatz MC, Lippman ZB** (2016) The
759 evolution of inflorescence diversity in the nightshades and heterochrony during
760 meristem maturation. Genome Res **26:** 1676–1686

761 **Lifschitz E, Eviatar T, Rozman A, Shalit A, Goldshmidt A, Amsellem Z, Alvarez JP,**
762 **Eshed Y** (2006) The tomato *FT* ortholog triggers systemic signals that regulate
763 growth and flowering and substitute for diverse environmental stimuli. Proc Natl Acad
764 Sci USA **103:** 6398–6403

765 **Liu C, Teo ZWN, Bi Y, Song S, Xi W, Yang X, Yin Z, Yu H** (2013) A Conserved Genetic
766 Pathway Determines Inflorescence Architecture in Arabidopsis and Rice. Dev Cell
767 **24:** 612–622

768 **Lück J, Lück HB, Bakkali M** (1990) A comprehensive model for acrotonic, mesotonic
769 and basitonic branchings in plants. Acta Biotheor **38:** 257–288

770 **Ma Q, Liu X, Franks RG, Xiang Q-Y** (2017) Alterations of *CorTFL1* and *CorAP1*
771 expression correlate with major evolutionary shifts of inflorescence architecture in

Cornus (Cornaceae) – a proposed model for variation of closed inflorescence forms. New Phytol **216:** 519–535

McGarry RC, Ayre BG (2012) Manipulation plant architecture with members of the CETS gene family. Plant Sci **188–189:** 71–81

Menzel CM (2019) Temperature has a greater effect on fruit growth than defoliation or fruit thinning in strawberries in the subtropics. Agriculture **9*:*** 127

Molinero-Rosales N, Jamilena M, Zurita S, Gómez P, Capel J, Lozano R (1999) *FALSIFLORA*, the tomato orthologue of *FLORICAULA* and *LEAFY*, controls flowering time and floral meristem identity. Plant J **20:** 685–693

Molinero-Rosales N, Latorre A, Jamilena M, Lozano R (2004) *SINGLE FLOWER TRUSS* regulates the transition and maintenance of flowering in tomato. Planta **218:** 427–434

Mouhu K, Hytönen T, Folta K, Rantanen M, Paulin L, Auvinen P, Elomaa P (2009) Identification of flowering genes in strawberry, a perennial SD plant. BMC Plant Biol **9:** 122

Nakano Y, Higuchi Y, Yoshida Y, Hisamatsu T (2015) Environmental responses of the FT/TFL1 gene family and their involvement in flower induction in *Fragaria* × *ananassa*. J Plant Physiol **177:** 60–66

Park SJ, Jiang K, Schatz MC, Lippman ZB (2012) Rate of meristem maturation determines inflorescence architecture in tomato. Proc Natl Acad Sci USA **109:** 639–644

Pnueli L, Carmel-Goren L, Hareven D, Gutfinger T, Alvarez J, Ganal M, Zamir D, Lifschitz E (1998) The *SELF-PRUNING* gene of tomato regulates vegetative to reproductive switching of sympodial meristems and is the ortholog of *CEN* and *TFL1*. Development **125:** 1979–1989

Peterson JL (1981) *Petri Net Theory and the Modeling of Systems*. Prentice-Hall, Englewood Cliffs

Prenner G, Vergara-Silva F, Rudall PJ (2009) The key role of morphology in modelling inflorescence architecture. Trends Plant Sci **14:** 302–309

Prusinkiewicz P, Erasmus Y, Lane B, Harder LD, Coen E (2007). Evolution and development of inflorescence architectures. Science **316:** 1452–1456

Prusinkiewicz P, Lindenmayer A (1990) *The Algorithmic Beauty of Plants*. With JS Hanan, FD Fracchia, D Fowler, MJM. de Boer and L Mercer. Springer, New York

Prusinkiewicz P, Remphrey W (2000) Characterization of architectural tree models using L-systems and Petri nets. In M. Labrecque, editor, *L'arbre — The Tree 2000: Papers presented at the 4th International Symposium on the Tree*, pp 177–186. Isabelle Quentin, Montreal

R Core Team (2021) R: A language and environment for statistical computing. R Foundation for Statistical Computing, Vienna, Austria. https://www.R-project.org/

Rantanen M, Kurokura T, Mouhu K, Pinho P, Tetri E, Halonen L, Palonen P, Elomaa P, Hytönen T (2014) Light quality regulates flowering in FvFT1/FvTFL1 dependent manner in the woodland strawberry *Fragaria vesca*. Front Plant Sci **5:** 271

Rantanen M, Kurokura T, Jiang P, Mouhu K, Hytönen T (2015) Strawberry homologue of TERMINAL FLOWER1 integrates photoperiod and temperature signals to inhibit flowering. Plant J **82:** 163 – 173

Quinet M, Dubois C, Goffin M-C, Chao J, Dielen V, Batoko H, Boutry M, Kinet J-M (2006) Characterization of tomato (*Solanum lycopersicum* L.) mutants affected in their flowering time and in the morphogenesis of their reproductive structure. J Exp Bot **57:** 1381–1390

Schultz EA, Haughn GW (1993) Genetic analysis of the floral initiation process (FLIP) in Arabidopsis. Development **119:** 745–765

Souer E, Rebocho AB, Bliek M, Kusters E, de Bruin RAM, Koes R (2008) Patterning of inflorescences and flowers by the F-Box protein DOUBLE TOP and the LEAFY homolog ABERRANT LEAF AND FLOWER of Petunia. Plant Cell **20:** 2033–2048

Thouet J, Quinet M, Lutts S, Kinet J-M, Périlleux C (2012) Repression of floral meristem fate is crucial in shaping tomato inflorescence. PloS One **7:** e31096–e31096

Weberling F (1989) *Morphology of flowers and inflorescences.* Cambridge University Press, Cambridge

Weigel D, Alvarez J, Smyth DR, Yanofsky MF, Meyerowitz EM (1992) LEAFY controls floral meristem identity in Arabidopsis. Cell **69:** 843–859

Weigel D, Meyerowitz ME (1993) Activation of floral homeotic genes in Arabidopsis. Science, **261:** 1723–1726

Zhang Y, Kan L, Hu S, Cheng L, Liu Z, Kang C (2022) The roles and evolution of the four LEAFY homologues in floral patterning and leaf development in woodland strawberry. BioRxiv, https://doi.org/10.1101/2022.10.06.511044

Zhu Y, Klasfeld S, Jeong CW, Jin R, Goto K, Yamaguchi N, Wagner D (2020) TERMINAL FLOWER 1-FD complex target genes and competition with FLOWERING LOCUS T. Nat Commun **11:** 5118

Zhu Y, Klasfeld S, Wagner D (2021) Molecular regulation of plant developmental transitions and plant architecture via PEPB family proteins: an update on mechanism of action. J Exp Bot **72:** 2301–2311

Parsed Citations

Alvarez J, Guli CL, Yu X-H, Smyth DR (1992) terminal flower: a gene affecting inflorescence development in Arabidopsis thaliana. Plant J 2: 103–116
Google Scholar: Author Only Title Only Author and Title

Anderson HM, Guttridge CG (1982) Strawberry truss morphology and the fate of high-order flower buds. Crop Research 22: 105–122
Google Scholar: Author Only Title Only Author and Title

Ashman TL, Hitchens MS (2000) Dissecting the causes of variation in intra-inflorescence allocation in a sexually polymorphic species, Fragaria virginiana (Rosaceae). Am J Bot 87: 197–204
Google Scholar: Author Only Title Only Author and Title

Bates D, Mächler M, Bolker B, Walker S (2015) Fitting linear mixed-effects models using lme4. J Stat Softw 67: 1–48
Google Scholar: Author Only Title Only Author and Title

Cieslak M, Khan N, Ferraro P, Soolanayakanahally R, Robinson SJ, Parkin I, McQuillan I, Prusinkiewicz P (2022) L-system models for image-based phenomics: case studies of maize and canola. isP 4: diab039
Google Scholar: Author Only Title Only Author and Title

Claßen-Bockhoff R, Bull-Hereñu K (2013) Towards an ontogenetic understanding of inflorescence diversity. Ann Bot 112: 1523–1542
Google Scholar: Author Only Title Only Author and Title

Corbesier L, Vincent C, Jang S, Fornara F, Fan Q, Searle I, Giakountis A, Farrona S, Gissot L, Turnbull C, Coupland G (2007) FT protein movement contributes to long-distance signaling in floral induction of Arabidopsis. Science 316: 1030–1033
Google Scholar: Author Only Title Only Author and Title

Darrow GM (1929) Inflorescence types of strawberry varieties. Am J Bot 16: 571–585
Google Scholar: Author Only Title Only Author and Title

Edger PP, VanBuren R, Colle M, Poorten TJ, Wai CM, Niederhuth CE, Alger EI, Ou S, Acharya CB, Wang J, Callow P, McKain MR, Shi J, Collier C, Xiong Z, Mower JP, Slovin JP, Hytönen T, Jiang N, Childs KL, Knapp SJ (2018) Single-molecule sequencing and optical mapping yields an improved genome of woodland strawberry (Fragaria vesca) with chromosome-scale contiguity. GigaScience 7: gix124
Google Scholar: Author Only Title Only Author and Title

Eshed Y, Lippman ZB (2019) Revolutions in agriculture chart a course for targeted breeding of old and new crops. Science 366: eaax0025
Google Scholar: Author Only Title Only Author and Title

Foster JC, Janick J (1969) Variable branching patterns in the strawberry inflorescence. J Am Soc Hortic Sci 94: 440–443
Google Scholar: Author Only Title Only Author and Title

Gleason HA, Cronquist A (1991) Manual of Vascular Plants of Northeastern United States and Adjacent Canada (2nd ed.). New York Botanical Garden
Google Scholar: Author Only Title Only Author and Title

Grimes J (1999) Inflorescence morphology, heterochrony, and phytogeny in the mimosoid tribes ingeae and acacieae (Leguminosae: Mimosoideae). Bot Rev 65: 317–347
Google Scholar: Author Only Title Only Author and Title

Guttridge CG (1985) Fragaria x ananassa. In AH Halevy ed, Handbook of Flowering, vol. 3. CRC Press, Boca Raton, FL, pp 16–33
Google Scholar: Author Only Title Only Author and Title

Harder LD, Jordan CY, Gross WE, Routley MB (2004) Beyond floricentrism: the pollination function of inflorescences. Plant Species Biol 19: 137–148
Google Scholar: Author Only Title Only Author and Title

Harder LD, Prusinkiewicz P (2013) The interplay between inflorescence development and function as the crucible of architectural diversity. Ann Bot 112: 1477–1493
Google Scholar: Author Only Title Only Author and Title

Hofmeister W (1868) Allgemeine Morphologie der Gewächse. In A de Bary, TH Irmisch, J Sachs, eds. Handbuch der Physiologischen Botanik. Engelmann, Leipzig, pp 405 – 664
Google Scholar: Author Only Title Only Author and Title

Jahn OL, Dana MN (1970) Crown and inflorescence development in the strawberry, Fragaria ananassa. Am J Bot 57: 605–612
Google Scholar: Author Only Title Only Author and Title

Kaneko-Suzuki M, Kurihara-Ishikawa R, Okushita-Terakawa C, Kojima C, Nagano-Fujiwara M, Ohki I, Tsuji H, Shimamoto K, Taoka KI (2018) TFL1-like proteins in rice antagonize rice FT-like protein in inflorescence development by competition for complex formation with 14-3-3 and FD. Plant Cell Physiol 59: 458–468
Google Scholar: Author Only Title Only Author and Title

Karwowski R, Prusinkiewicz P (2003) Design and implementation of the L+C modeling language. Electron Notes Theor Comput Sci 86: 134–152
Google Scholar: Author Only Title Only Author and Title

Kellogg EA (2000) A model of inflorescence development. In KL Wilson and DA Morrison eds, Monocots: Systematics and Evolution. CSIRO, Melbourne, pp 84–88.
Google Scholar: Author Only Title Only Author and Title

Kobayashi K, Yasuno N, Sato Y, Yoda M, Yamazaki R, Kimizu M, Yoshida H, Nagamura Y, Kyozuka J (2012) Inflorescence meristem identity in rice is specified by overlapping functions of three AP1/FUL-Like MADS box genes and PAP2, a SEPALLATA MADS box gene. Plant Cell 24: 1848–1859
Google Scholar: Author Only Title Only Author and Title

Koskela EA, Mouhu K, Albani MC, Kurokura T, Rantanen M, Sargent DJ, Battey NH, Coupland G, Elomaa P, Hytönen T (2012) Mutation in TERMINAL FLOWER1 reverses the photoperiodic requirement for flowering in the wild strawberry Fragaria vesca. Plant Physiol 159: 1043–1054
Google Scholar: Author Only Title Only Author and Title

Koskela EA, Kurokura T, Toivainen T, Sønsteby A, Heide OM, Sargent DJ, Isobe S, Jaakola L, Hilmarsson H, Elomaa P, Hytönen T (2017) Altered regulation of TERMINAL FLOWER 1 causes the unique vernalisation response in an arctic woodland strawberry accession. New Phytol 216: 841–853
Google Scholar: Author Only Title Only Author and Title

Kurokura T, Samad S, Koskela E, Mouhu K, Hytönen T (2017) Fragaria vesca CONSTANS controls photoperiodic flowering and vegetative development. J Exp Bot 68: 4839–4850
Google Scholar: Author Only Title Only Author and Title

Lee C, Kim S-J, Jin S, Susila H, Youn G, Nasim Z, Alavilli H, Chung K-S, Yoo SJ, Ahn JH (2019) Genetic interactions reveal the antagonistic roles of FT/TSF and TFL1 in the determination of inflorescence meristem identity in Arabidopsis. Plant J 99: 452–464
Google Scholar: Author Only Title Only Author and Title

Lemmon ZH, Park SJ, Jiang K, Van Eck J, Schatz MC, Lippman ZB (2016) The evolution of inflorescence diversity in the nightshades and heterochrony during meristem maturation. Genome Res 26: 1676–1686
Google Scholar: Author Only Title Only Author and Title

Lifschitz E, Eviatar T, Rozman A, Shalit A, Goldshmidt A, Amsellem Z, Alvarez JP, Eshed Y (2006) The tomato FT ortholog triggers systemic signals that regulate growth and flowering and substitute for diverse environmental stimuli. Proc Natl Acad Sci USA 103: 6398–6403
Google Scholar: Author Only Title Only Author and Title

Liu C, Teo ZWN, Bi Y, Song S, Xi W, Yang X, Yin Z, Yu H (2013) A Conserved Genetic Pathway Determines Inflorescence Architecture in Arabidopsis and Rice. Dev Cell 24: 612–622
Google Scholar: Author Only Title Only Author and Title

Lück J, Lück HB, Bakkali M (1990) A comprehensive model for acrotonic, mesotonic and basitonic branchings in plants. Acta Biotheor 38: 257–288
Google Scholar: Author Only Title Only Author and Title

Ma Q, Liu X, Franks RG, Xiang Q-Y (2017) Alterations of CorTFL1 and CorAP1 expression correlate with major evolutionary shifts of inflorescence architecture in Cornus (Cornaceae) – a proposed model for variation of closed inflorescence forms. New Phytol 216: 519–535
Google Scholar: Author Only Title Only Author and Title

McGarry RC, Ayre BG (2012) Manipulation plant architecture with members of the CETS gene family. Plant Sci 188–189: 71–81
Google Scholar: Author Only Title Only Author and Title

Menzel CM (2019) Temperature has a greater effect on fruit growth than defoliation or fruit thinning in strawberries in the subtropics. Agriculture 9: 127
Google Scholar: Author Only Title Only Author and Title

Molinero-Rosales N, Jamilena M, Zurita S, Gómez P, Capel J, Lozano R (1999) FALSIFLORA, the tomato orthologue of FLORICAULA and LEAFY, controls flowering time and floral meristem identity. Plant J 20: 685–693
Google Scholar: Author Only Title Only Author and Title

Molinero-Rosales N, Latorre A, Jamilena M, Lozano R (2004) SINGLE FLOWER TRUSS regulates the transition and maintenance

of flowering in tomato. Planta 218: 427–434
Google Scholar: Author Only Title Only Author and Title

Mouhu K, Hytönen T, Folta K, Rantanen M, Paulin L, Auvinen P, Elomaa P (2009) Identification of flowering genes in strawberry, a perennial SD plant. BMC Plant Biol 9: 122
Google Scholar: Author Only Title Only Author and Title

Nakano Y, Higuchi Y, Yoshida Y, Hisamatsu T (2015) Environmental responses of the FT/TFL1 gene family and their involvement in flower induction in Fragaria × ananassa. J Plant Physiol 177: 60–66
Google Scholar: Author Only Title Only Author and Title

Park SJ, Jiang K, Schatz MC, Lippman ZB (2012) Rate of meristem maturation determines inflorescence architecture in tomato. Proc Natl Acad Sci USA 109: 639–644
Google Scholar: Author Only Title Only Author and Title

Pnueli L, Carmel-Goren L, Hareven D, Gutfinger T, Alvarez J, Ganal M, Zamir D, Lifschitz E (1998) The SELF-PRUNING gene of tomato regulates vegetative to reproductive switching of sympodial meristems and is the ortholog of CEN and TFL1. Development 125: 1979–1989
Google Scholar: Author Only Title Only Author and Title

Peterson JL (1981) Petri Net Theory and the Modeling of Systems. Prentice-Hall, Englewood Cliffs
Google Scholar: Author Only Title Only Author and Title

Prenner G, Vergara-Silva F, Rudall PJ (2009) The key role of morphology in modelling inflorescence architecture. Trends Plant Sci 14: 302–309
Google Scholar: Author Only Title Only Author and Title

Prusinkiewicz P, Erasmus Y, Lane B, Harder LD, Coen E (2007). Evolution and development of inflorescence architectures. Science 316: 1452–1456
Google Scholar: Author Only Title Only Author and Title

Prusinkiewicz P, Lindenmayer A (1990) The Algorithmic Beauty of Plants. With JS Hanan, FD Fracchia, D Fowler, MJM. de Boer and L Mercer. Springer, New York
Google Scholar: Author Only Title Only Author and Title

Prusinkiewicz P, Remphrey W (2000) Characterization of architectural tree models using L-systems and Petri nets. In M. Labrecque, editor, L'arbre - The Tree 2000: Papers presented at the 4th International Symposium on the Tree, pp 177–186. Isabelle Quentin, Montreal
Google Scholar: Author Only Title Only Author and Title

R Core Team (2021) R: A language and environment for statistical computing. R Foundation for Statistical Computing, Vienna, Austria. https://www.R-project.org/
Google Scholar: Author Only Title Only Author and Title

Rantanen M, Kurokura T, Mouhu K, Pinho P, Tetri E, Halonen L, Palonen P, Elomaa P, Hytönen T (2014) Light quality regulates flowering in FvFT1/FvTFL1 dependent manner in the woodland strawberry Fragaria vesca. Front Plant Sci 5: 271
Google Scholar: Author Only Title Only Author and Title

Rantanen M, Kurokura T, Jiang P, Mouhu K, Hytönen T (2015) Strawberry homologue of TERMINAL FLOWER1 integrates photoperiod and temperature signals to inhibit flowering. Plant J 82: 163 – 173
Google Scholar: Author Only Title Only Author and Title

Quinet M, Dubois C, Goffin M-C, Chao J, Dielen V, Batoko H, Boutry M, Kinet J-M (2006) Characterization of tomato (Solanum lycopersicum L.) mutants affected in their flowering time and in the morphogenesis of their reproductive structure. J Exp Bot 57: 1381–1390
Google Scholar: Author Only Title Only Author and Title

Schultz EA, Haughn GW (1993) Genetic analysis of the floral initiation process (FLIP) in Arabidopsis. Development 119: 745–765
Google Scholar: Author Only Title Only Author and Title

Souer E, Rebocho AB, Bliek M, Kusters E, de Bruin RAM, Koes R (2008) Patterning of inflorescences and flowers by the F-Box protein DOUBLE TOP and the LEAFY homolog ABERRANT LEAF AND FLOWER of Petunia. Plant Cell 20: 2033–2048
Google Scholar: Author Only Title Only Author and Title

Thouet J, Quinet M, Lutts S, Kinet J-M, Périlleux C (2012) Repression of floral meristem fate is crucial in shaping tomato inflorescence. PloS One 7: e31096–e31096
Google Scholar: Author Only Title Only Author and Title

Weberling F (1989) Morphology of flowers and inflorescences. Cambridge University Press, Cambridge
Google Scholar: Author Only Title Only Author and Title

Weigel D, Alvarez J, Smyth DR, Yanofsky MF, Meyerowitz EM (1992) LEAFY controls floral meristem identity in Arabidopsis. Cell 69: 843–859
Google Scholar: Author Only Title Only Author and Title

Weigel D, Meyerowitz ME (1993) Activation of floral homeotic genes in Arabidopsis. Science, 261: 1723–1726
Google Scholar: Author Only Title Only Author and Title

Zhang Y, Kan L, Hu S, Cheng L, Liu Z, Kang C (2022) The roles and evolution of the four LEAFY homologues in floral patterning and leaf development in woodland strawberry. BioRxiv, https://doi.org/10.1101/2022.10.06.511044
Google Scholar: Author Only Title Only Author and Title

Zhu Y, Klasfeld S, Jeong CW, Jin R, Goto K, Yamaguchi N, Wagner D (2020) TERMINAL FLOWER 1-FD complex target genes and competition with FLOWERING LOCUS T. Nat Commun 11: 5118
Google Scholar: Author Only Title Only Author and Title

Zhu Y, Klasfeld S, Wagner D (2021) Molecular regulation of plant developmental transitions and plant architecture via PEPB family proteins: an update on mechanism of action. J Exp Bot 72: 2301–2311
Google Scholar: Author Only Title Only Author and Title